processes

MDPI

Article

Numerical Analysis and Optimization of Solar-Assited Heat Pump Drying System with Waste Heat Recovery Based on TRNSYS

Zhiyuan Xie [1,2,3,4], Yulie Gong [1,2,3,*], Cantao Ye [1,2,3], Yuan Yao [1,2,3] and Yubin Liu [1,2,3]

1 Guangzhou Institute of Energy Conversion, Chinese Academy of Sciences, Guangzhou 510640, China; xiezy@ms.giec.ac.cn (Z.X.); yect@ms.giec.ac.cn (C.Y.); yaoyuan@ms.giec.ac.cn (Y.Y.); Liuyb@ms.giec.ac.cn (Y.L.)
2 CAS Key Laboratory of Renewable Energy, Guangzhou 510640, China
3 Guangdong Provincial Key Laboratory of New and Renewable Energy Research and Development, Guangzhou 510640, China
4 University of Chinese Academy of Sciences, Beijing 100049, China
* Correspondence: gongyl@ms.giec.ac.cn

Abstract: In this paper, a new solar-assisted heat pump drying system with waste heat recovery and double water tanks (SCAHP) was established and the system optimized by TRNSYS and variable air volume experiment. The annual cumulative efficiency of the SCAHP (COP_{ac}), buffer tank heating efficiency (η_{BT}) and hot water storage tank heating efficiency (η_{ST}) are all considered as optimization objectives, and this paper discusses the relationship between the three optimization objectives and studies the influence of hot air volume (q_{DR}), area of solar collector (A_{SC}), inclination angle of solar collector (I_{SC}) and volume of heat storage water tank (V_{ST}) on system efficiency in the drying process. In order to explore the general rule of system optimization, numerical analysis and optimization were carried out in five typical cities in five climatic regions of China. The results show that the mixed variable air volume mode can increase the drying rate with less energy loss, and shorten the drying period by 28.6–33.3%. When the system surface body ratio (SBR) in Nanjing is between 3.1 and 4.1, the COP_{ac}, η_{BT}, and η_{ST} can reach the maximum value simultaneously. It is estimated that the cost can be recovered in 5 years when the system configuration parameters are optimized.

Keywords: solar assisted heat pump drying; numerical simulation; system configuration optimization

Citation: Xie, Z.; Gong, Y.; Ye, C.; Yao, Y.; Liu, Y. Numerical Analysis and Optimization of Solar-Assited Heat Pump Drying System with Waste Heat Recovery Based on TRNSYS. *Processes* **2021**, *9*, 1118. https://doi.org/10.3390/pr9071118

Academic Editor: Alfredo Iranzo

Received: 2 June 2021
Accepted: 19 June 2021
Published: 28 June 2021

1. Introduction

Drying has a large number of applications in industry, agriculture and other fields, while drying is one of the most energy-consuming units [1]. In developed countries, about 10% of fuel is used for drying, and in China, drying energy consumption accounts for about 12% of the entire industrial energy consumption [2]. In some industries, the energy waste caused by drying is enormous, with Mujumdar [3] reporting that drying consumes up to 70% of the total energy in the manufacture of wood products, 50% of the total energy in the manufacture of finished textiles, and over 60% of the total energy in agricultural maize production. In order to develop sustainable energy sources, three important technological changes are required: energy conservation on the demand side, increased efficiency in energy production, and the replacement of fossil fuels with various renewable sources [4]. In this regard, the use of heat pump drying systems and solar heat collecting systems has improved energy efficiency and reduced consumption of fossil fuels.

The energy efficiency of traditional dryers is usually very low. Lawton J [5] points out that the efficiency of traditional dryers can only reach 35% at the highest. Queiroz R [6] found that heat pump drying saves 40% energy in comparison with using electrical heater dryers. The traditional dryer is not only inefficient, but also the quality of drying products

is not up to the requirements. With the rapid development of industry and agriculture, vacuum drying, freeze drying, spray drying and other methods have been put forward one after another; however, these drying processes are highly energy-intensive and have the disadvantages of high economic costs or low drying rates, and the advantages of heat pump drying are further prominent. In some studies, heat pump drying is considered to provide better product quality under the premise of lower energy consumption [7–11]. The first batch of heat pump drying studies in the literature was completed by Hodgett [12] and Geeraert [13]. In recent decades, many scientists have studied how to improve the efficiency of heat pump systems from various aspects [14–16]. However, related studies show that heat pump technology still has problems such as using high-grade electric energy, the small drying scale of single heat pumps and high system maintenance costs [17,18].

The combination of multiple energy sources, especially the introduction of renewable energy, has become one of the current research hotspots. Solar energy has attracted much attention as the most readily available renewable energy source. Open solar drying is the earliest drying technology that has been applied [19], but its external drying conditions are difficult to be controlled, resulting in too-long drying times of materials or poor quality of dried products. The efficiency of solar direct drying of crops is between 20–40% [20]. To solve these problems, many scientists are trying to combine solar drying with heat pump technology.

Luo Huilong et al . [21] designed and constructed an air source heat pump-assisted solar energy drying system. Compared with conventional drying systems, the air source heat pump-assisted solar energy drying system has greater energy saving potential. Rahman et al . [22] economically optimized the evaporator and air collector of a solar-assisted heat pump drying system. Their economic analysis showed that using an air collector area of 1.25 m^2 and an evaporator collector area of 2 m^2, the system had significant cost savings with a payback period of 4.4 years. In a recent work, Meltem [23] et al . designed and tested a new type of sustainable photovoltaic/heat-assisted heat pump drying. The results show that the average coefficient of performance of the heat pump can reach 4.18, according to solar radiation and ambient temperature, and an average electric efficiency of 12.27% and a maximum of 14.02% can be obtained.

However, in the drying system combined with solar energy and heat pump, there is often a mismatch between energy supply and demand and excessive waste heat waste. Energy storage technology can solve this problem well. The application of heat storage in the solar drying system is justified under the following three circumstances [24]: (1) the drying period can be prolonged by energy storage; (2) the excess energy at the peak of radiation can be stored to avoid excessive local drying; and (3) the temperature of dry air can be controlled to avoid damage to materials. Qiu et al . [25] used a solar-assisted heat pump drying system with heat recovery to dry 10 kg of carrots, and the results showed that the system saved about 40.5% of the energy. Wang et al . [26] studied the use of another form of solar-assisted heat pump drying system with heat recovery to dry 80 kg of mangoes, and the results showed that the efficiency of the system was improved by about 6%, and the waste heat recovery rate reached 41.7%.

On the basis of predecessors' research, this paper proposes a new solar-assisted heat pump drying system with waste heat recovery and double water tanks, where the waste heat recovery module can partially offset the variable air volume of energy loss. On the basis of experiment explores the influence of variable air volume on the drying process, and system efficiency, the whole-year numerical simulation is carried out based on TRNSYS, and the parameters and operation parameters of each component of the system are optimized.

2. System Model and Research Method

2.1. Introduction of SCAHP

Figure 1 shows the schematic diagram of SCAHP. The system includes a solar collector (SC), air-water heat exchanger (AWEH), buffer tank (BT), hot water storage tank (ST),

air-water heat pump (HP), water pump, fan and drying room (DR). The parameters of system components, operation parameters and corresponding variation ranges are shown in Table 1. Among them, the fan is a forced convection fan installed at the outlet of DR, so as to facilitate the variable air volume drying experiment and waste heat recovery.

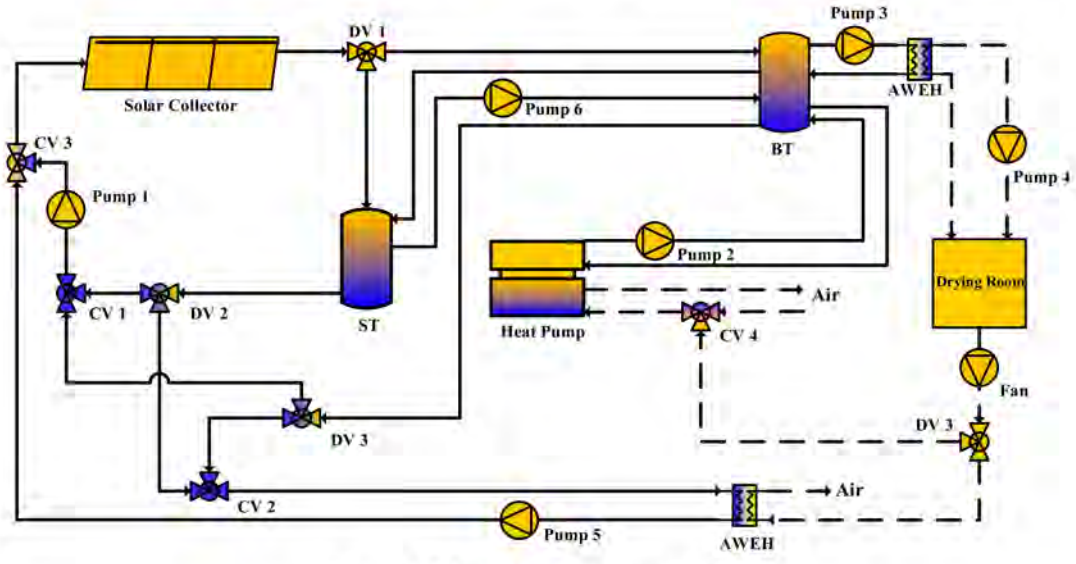

Figure 1. Schematic diagram of SCAHP.

Table 1. Characteristics of the instruments.

Name	Reference Value	Range
I_{SC}	30°	15°~50°
A_{SC}	0.3 m^2	0.1 m^2~0.8 m^2
SC Efficiency	Optional efficency: 0.8, heat loss coefficient: 0.78 W/(m^2·°C)	–
V_{BT}	0.05 m^3	–
V_{ST}	0.04 m^3	0.2 m^3~0.4 m^3
HP	Output = 1.5 kW	–
Pump 1 flow	21 kg/h	–
Pump 3 flow	250 kg/h	–

All energy consumption of DR is provided by BT, the heat of BT comes from SC, HP, ST and waste heat recovery, the heat of ST comes from the SC and waste heat recovery, and the heat recovered from waste heat can be used in two ways: first, passing the waste hot air directly to the low temperature side of the HP through the fan; second, passing the waste hot air to the SC inlet side after being converted by AWEH.

The SC and HP are connected in parallel, and the start and stop of the SC circuit is not directly related to the start and stop of the HP circuit. When the temperature of the BT is insufficient, the SC is first opened for heating, that is, pump 1 is turned on, and priority is given to the heat supply to the BT. The above can be expressed as that the hot water in the SC flows to the BT through DV 1, and then flows back to the SC through DV 3, CV 1, Pump 1, and CV 3 after coming out of the BT. When the temperature of the BT reaches the set value, but the temperature of the ST does not reach the set value, the hot water in the SC flows to the ST through DV 1, and passes through DV 2, CV 1, Pump 1 and CV 3 after coming out of the ST flow back to the SC. When the temperature of the BT and ST reach the set value, the SC circuit is closed. When the temperature in the BT is lower than a set value lower than the set temperature of the SC circuit, the HP and Pump 2 are turned on, and the hot water flows into the BT and returns to the HP until the BT reaches the set upper limit and closes the loop.

Waste heat recovery can be achieved by passing the waste heat to the inlet of the SC or the low temperature side of the HP through the fan. There are two points to note: 1, the carrier of waste heat recovery heat is air. When it leads to the low temperature side of the SC, it needs to be converted by a water-air heat exchanger. At the inlet of the SC, it is mixed with the return water of the original SC circuit, heated by the SC, and then led to the BT or ST. 2, When the heat recovered by the waste heat directly passes to the low temperature side of the HP, it may not be able to meet the flow demand of the low temperature side of the HP. At this time, the hot air from the waste heat recovery needs to be mixed with the air in the atmospheric environment, that is, pass through CV 4 to the low temperature side of the HP.

The heat supply from the ST to the BT is only related to the temperature difference between the two water tanks, and whether the BT reaches the set temperature is related. From the perspective of heat supply, the heat supply from the ST is in parallel with the heat supplied by the SC and HP. When the heating conditions are met, pump 6 is turned on, and the hot water flows from the ST to the BT and returns to the ST. It should be noted that the control logic of this system and the set temperature range of each loop will be described in detail in Section 2.2 Control Logic.

2.2. Control Logic of SCAHP

Figure 2a,b are combined to show the complete control logic of SCAHP. Figure 2a shows the control logic of SCAHP except for the waste heat recovery module. The figure also provides the temperature settings of the water tank in each heating mode mentioned in Section 2.1. According to the temperature value of the BT, the control mode of the system is divided into three modes.

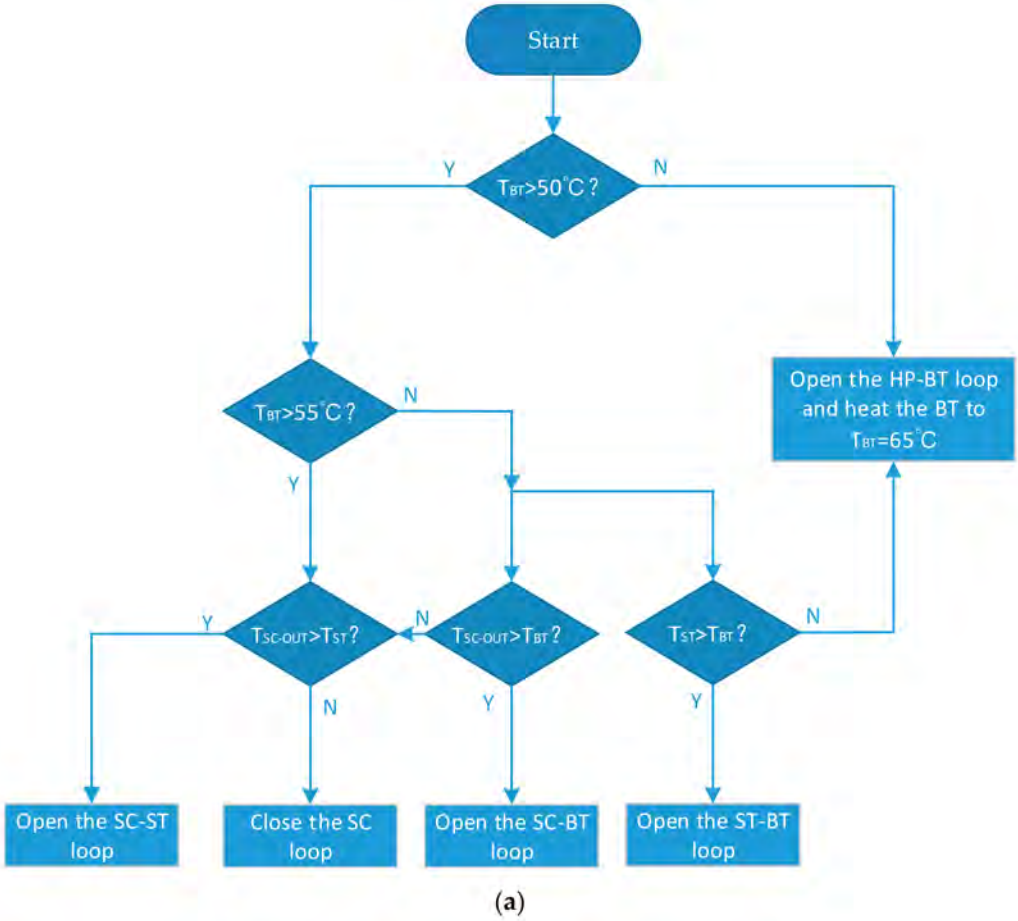

Figure 2. *Cont.*

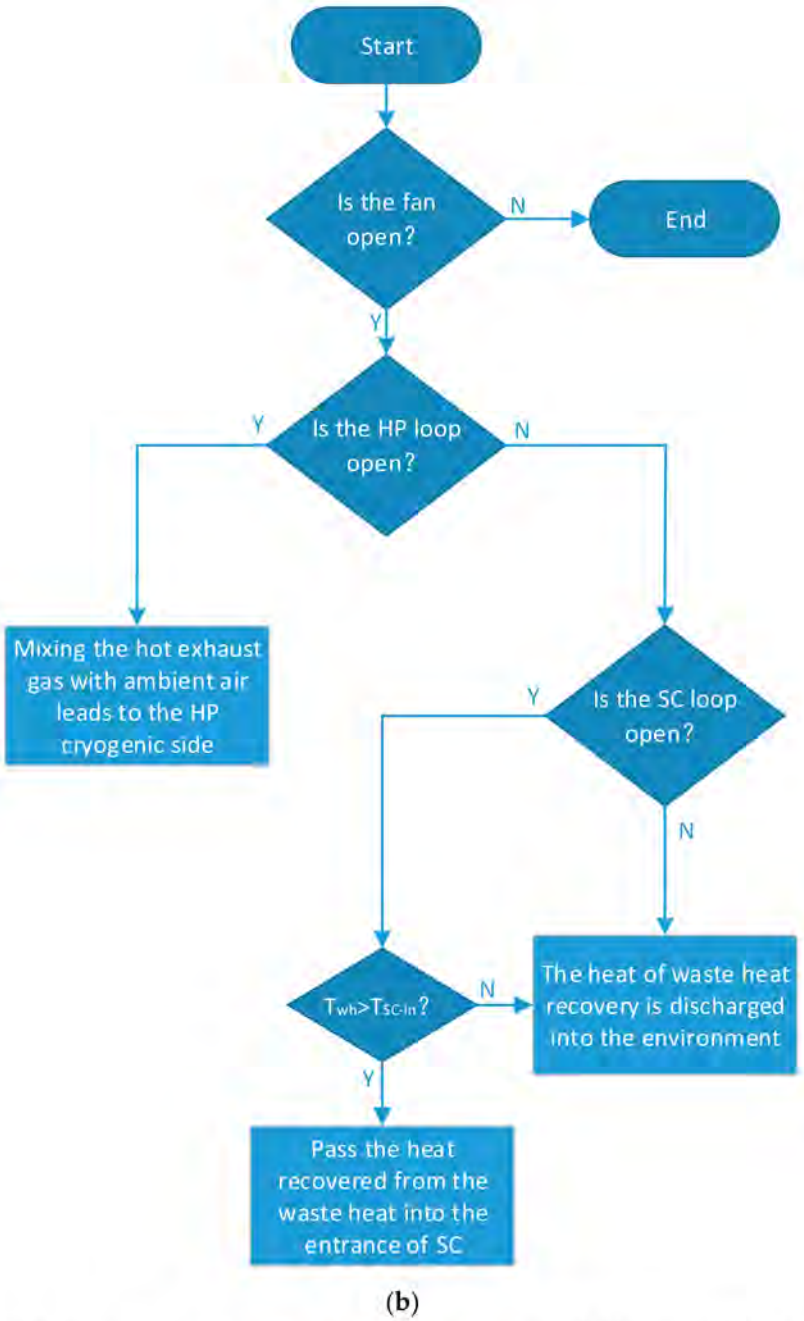

Figure 2. (**a**) SCAHP operation logic, part 1: the control logic of SCAHP except for the waste heat recovery module. (**b**) SCAHP operation logic, part 2: the control logic of the waste heat recovery module.

Mode 1: If the average temperature of BT (T_{BT}) is lower than 50 °C, turn on the HP to heat the BT to 65 °C, and then turn off the HP. At the same time, it is judged whether the outlet temperature of SC ($T_{SC\text{-}OUT}$) or the outlet temperature of ST (T_{ST}) is greater than T_{BT}. When the judgment value is 1, the heating circuit of the SC or ST is started to heat the BT to 55 °C. When T_{BT} reaches 55 °C or $T_{SC\text{-}OUT}$ is less than T_{BT}, judge whether $T_{SC\text{-}OUT}$ is greater than T_{ST}. When the judgment value is 1, the SC transfers heat to the ST.

Mode 2: When T_{BT} is greater than 50 °C and less than 55 °C, it is judged whether $T_{SC\text{-}OUT}$ or T_{ST} is greater than T_{BT}. When the judgment value is 1, the SC or ST is activated to transfer heat to the BT until T_{BT} gets to 55 °C, When T_{BT} reaches 55 °C or $T_{SC\text{-}OUT}$ is less than T_{BT}, judge whether $T_{SC\text{-}OUT}$ is greater than T_{ST}. When the judgment value is 1, the

SC is started to transfer heat to the ST, otherwise SCAHP is in shutdown state, and T_{BT} gradually drops and enters mode 1.

Mode 3: When the temperature of the BT is greater than 55 °C, it is judged whether the outlet temperature of the SC is greater than the temperature of the ST. When the judgment value is 1, the SC will be started for heating, otherwise the system is in shutdown state, and the temperature of the BT will gradually drop into mode 2.

Figure 2b shows the control logic of the system's waste heat recovery module. The first thing to note is that when the waste heat recovery fan is not turned on, the waste heat mode is turned off and the system does not enter this control module. When the fan is turned on, first determine whether the HP is turned on. When the HP is turned on, the hot air obtained in the waste heat recovery and ambient air will be mixed and sent to the low temperature side of the HP. If the HP is in a shutdown state, judge whether the SC circuit is open, and whether the temperature of the hot water exchanged with the hot air recovered by the waste heat in the heat exchanger is greater than the inlet temperature of the SC; when the two judgments both return the value 1, the heat recovered by the waste heat is led to the entrance of the SC, otherwise the waste heat is directly discharged into the surrounding environment.

2.3. TRNSYS Simulation Model of SCAHP

According to the SCAHP physical model, control logic and parameter settings described above, a system simulation model is established in TRNSYS 17. TRNSYS (Transient System Simulation Program) is an extremely flexible graphically based software environment used to simulate the behavior of transient systems, and most TRNSYS-based simulations focus on evaluating the performance of thermal and electrical energy systems. The model contains weather file, SC, HP, BT, ST, DR, water pump, fan, heat exchanger and control strategy. The main components of the TRNSYS simulation model and their descriptions are shown in Table 2.

Table 2. Main component in TRNSYS.

Name	Component Type	Descriptions
Weather data	Type 152	This component serves the purpose of reading data at regular time intervals from an external weather data file
Tank	Type 4	Thermal storage device
Heat pump	Type 941	This component models a single-stage air to water heat pump
pump	Type 114	Type114 models a single (constant) speed pump that is able to maintain a constant fluid outlet mass flow rate
Flow diverter	Type 649/11f	Two inlet liquid flows are mixed into a single liquid outlet flow
Flow mixer	Type 11h	A single inlet liquid outlet flow is divided into two outlet liquids
Temperature judgement	Type 2b	The on/off differential controller generates a control function which can have a value of 1 or 0.
Drying room	Type 682	This model simply imposes a user-specified load (cooling = positive load, heating = negative load) on a flow stream and calculates the resultant outlet fluid conditions.

When performing model verification, the time step is set to 1 min, which is controlled at the same magnitude as the time step of the verification object. In the simulation analysis of the whole year, the step length is set to 1 h. The system control strategy is implemented by Type 2b and calculator. The shunt valve at the outlet of the BT and ST is replaced by a calculator. The TRNSYS simulation model diagram is shown in Figure 3.

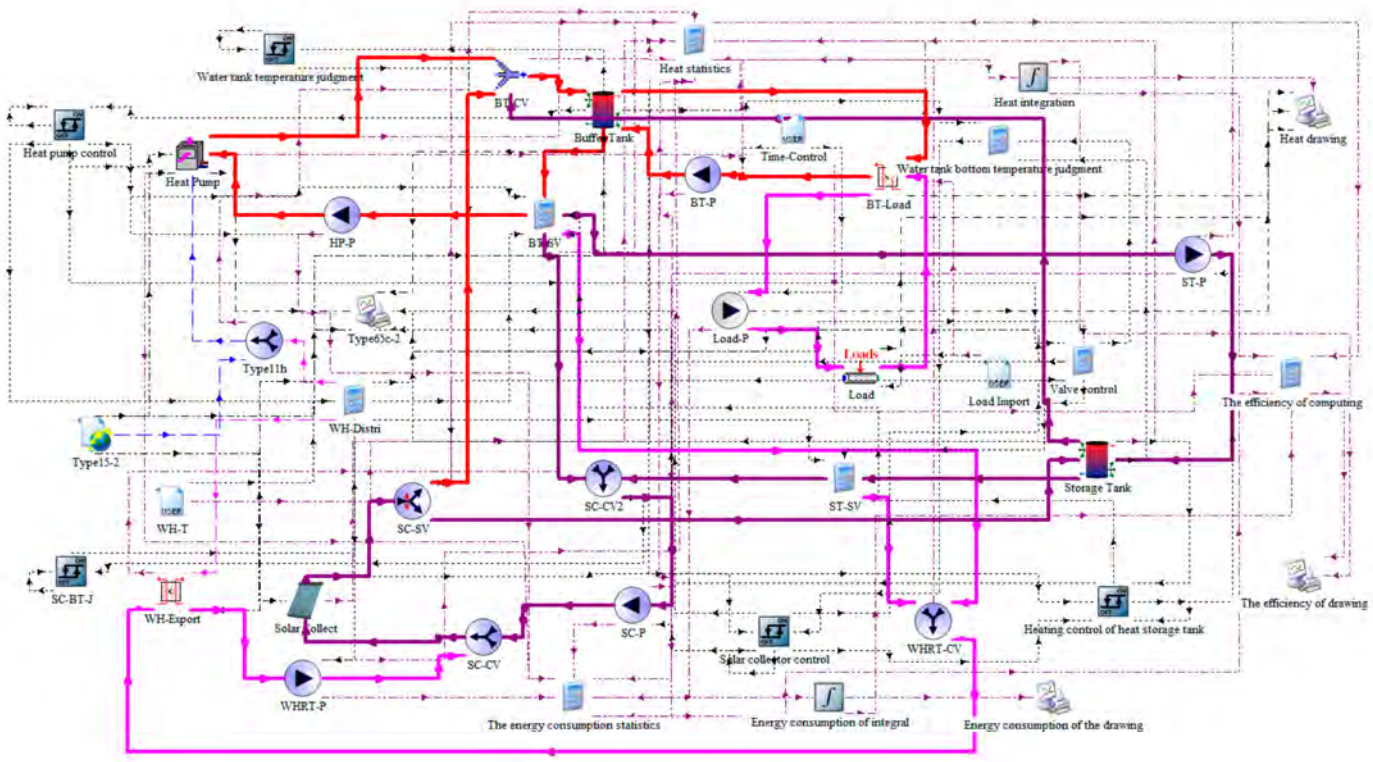

Figure 3. TRNSYS model of SCAHP.

2.4. Research Method

This research adopts a combination of experiment and simulation, taking 731 g of carrots as the experimental material, and exploring the influence of variable air volume on material drying, suitable variable air volume control modes, drying rate and energy consumption data of different variable air volume modes in the variable air volume experiment. Exploring the optimal configuration and optimal operating parameters of the system in the simulation, input of the real-time data of the DR energy consumption is obtained through the experiment through Type 682. Taking COP_{ac}, η_{BT} and η_{ST} as optimization goals, orthogonal experiments are used to optimize A_{SC}, I_{SC} and V_{ST}. Finally, the economic performance of the system is also verified.

This study takes five typical cities in China's five major climate regions as the research objects, namely Harbin, Tianjin, Nanjing, Guangzhou, and Kunming, to explore the general laws of the system proposed in this paper. In the simulation calculation, the meteorological parameters are based on the typical yearly parameters of five cities. The typical meteorological year (TMY) is based on the monthly average of the past 10 years. The parameters of the five cities are shown in Table 3. Taking Nanjing City as the main analysis object, the analysis and optimization results of other cities will be summarized in the table and given uniformly. It should be pointed out that in our model only the difference in ambient temperature and solar radiation between different cities is considered.

Table 3. Basic Parameters of Typical Cities in Five Climate Zones of China.

Name	Climate Region	Longitude(°)	Latitude(°)	Average Temperature of the Coldest Month (°C)	Average Temperature of the Hottest Month (°C)
Harbin	Severe cold area	126.77	45.75	−16.9	23.8
Tianjin	Cold area	117.17	39.93	−2.9	27.1
Nanjing	Hot summer and cold winter area	118.80	32.00	3.1	28.3
Guangzhou	Hot summer and warm winter area	113.33	23.17	14.3	28.8
Kunming	Temperate area	102.65	25.00	9.4	20.3

3. Mathematical Model

3.1. Total Heat Required for Drying Process

The heat consumed by carrots during the drying process can be divided into three parts: The heat required for preheating carrots, the heat required for evaporation of water from carrots, and the heat loss of the entire system during the drying process. According to the first law of thermodynamics:

$$Q_t = Q_p + Q_e + Q_l \tag{1}$$

The heat required for the carrot preheating stage is:

$$Q_p = c_r m_{r0}(T_{r1} - T_{r0}) \tag{2}$$

where c_r is the specific heat of the carrot under constant pressure (kJ/kg·k), m_{r0} is the initial mass of the carrot (kg), and T_{r0} is the carrot temperature before preheating (°C), equivalent to ambient temperature, and T_{r1} is the carrot temperature after preheating (°C), equivalent to the temperature after the constant temperature of the DR stabilizes.

The heat required by carrots to evaporate water is:

$$Q_e = \gamma \cdot (m_{r0} - m_{r2}) \tag{3}$$

where γ is the latent heat of vaporization of the moisture in the carrot (kJ/kg), and m_{r2} is the mass of the carrot after the drying (kg).

The heat loss during the drying process of carrot is:

$$Q_l = (Q_p + Q_e) \times 10\% \tag{4}$$

3.2. Solar Collector

The total amount of radiation during the working hours of SC is:

$$G = 3.6 \int_0^{t_1} A_c I_t dt \tag{5}$$

where A_c is the area of the solar collector (m^2), I_t is the instantaneous solar radiation value incident on the SC, W/m^2, and t_1 is the total open time of the SC (h).

The energy used by the SC to provide the DR is:

$$Q_{sc} = \eta_{BT}\eta_{AWHE}[G \cdot \eta_{sc} + (\eta_{ST} - 1) \times Q_{SC-ST}] \tag{6}$$

where G is the total energy received by the SC (kJ), η_{sc} is the conversion efficiency of SC, η_{BT} is the heating efficiency of the BT, η_{ST} is the heating efficiency of the ST, η_{AWHE} is the heat exchange efficiency of the air-water heat exchanger, the air-water heat exchange efficiency of the system is set to a fixed value, 0.65, and Q_{SC-ST} is the total energy obtained by the ST from the SC (kJ).

The total heating share (SF) of the system occupied by the heat supply of solar collectors can be expressed as:

$$SF = Q_{sc}/Q_t \tag{7}$$

3.3. Tank

The heat supplied by the SC to the BT is:

$$Q_{SC-BT} = 3600 \int_0^{t_2} m_{sc} c_{sc} (T_{scout} - T_{scin}) dt \tag{8}$$

The heat supplied by the SC to the ST is:

$$Q_{SC-ST} = 3600 \int_0^{t_3} m_{sc} c_{sc} (T_{scout} - T_{scin}) dt \tag{9}$$

where m_{sc} is the mass flow of water passing through the solar collector (kg/s), c_{sc} is the specific heat of water under constant pressure kJ/kg·k, and T_{scout} is the outlet temperature of the SC (°C), T_{scin} is the inlet temperature of the SC (°C), t_2 is the time it takes for SC to supply heat to the BT (h), t_3 is the time it takes for the SC to supply heat to the ST (h).

The heat supplied by the HP to the BT is:

$$Q_{HP-BT} = 3600 \int_0^{t_4} m_{HP} c_{HP} (T_{HPout} - T_{HPin}) dt \tag{10}$$

where m_{HP} is the mass flow of water passing through HP (kg/s), c_{HP} is the specific heat of water under constant pressure (kJ/kg·k), and T_{HPout} is the outlet temperature on the condenser side of the HP (°C), T_{HPin} is the inlet temperature on the condenser side of the HP (°C), t_4 is the total open time of the HP (h).

The heat supplied by the ST to the BT is:

$$Q_{ST-BT} = 3600 \int_0^{t_5} m_{HB} c_{HB} (T_{HBout} - T_{HBin}) dt \tag{11}$$

where m_{HB} is the mass flow rate of water flowing from the ST to the BT (kg/s), c_{HB} is the specific heat of water under constant pressure (kJ/kg·k), and T_{HBin} is the outlet temperature of the ST flowing to the BT (°C), T_{HBout} is the outlet temperature of the BT flowing to the ST (°C), t_5 is the time it takes for the ST to supply heat to the BT (h).

The heat obtained by the BT is:

$$Q_{SC/HP/ST-BT} = Q_{SC-BT} + Q_{HP-BT} + Q_{ST-BT} \tag{12}$$

The heat supplied by BT to DR is:

$$Q_{BT-DR} = 3600 \int_0^{t_6} m_{BD} c_{BD} (T_{BDin} - T_{BDout}) dt \tag{13}$$

where m_{BD} is the mass flow of water from the BT to the air-water heat exchanger connected to the DR (kg/s), and c_{BD} is the specific heat of water under constant pressure (kJ/kg·k), T_{BDin} is the outlet water temperature of the BT flowing to the air-water heat exchanger connected to the DR (°C), T_{BDout} is the temperature entering the BT from the air-water heat exchanger connected to the DR (°C), and t_6 is the time it takes for the BT to supply heat to the DR (h).

The heating efficiency of the SC is:

$$\eta_{sc} = (Q_{SC-HWTS} + Q_{SC-BT}) / \left(3.6 \int_0^t A_c I_t dt\right) \tag{14}$$

The heating efficiency of the BT is:

$$\eta_{BT} = Q_{BT-DR}/Q_{SC/HP/ST-BT} \tag{15}$$

The heating efficiency of the ST is:

$$\eta_{ST} = Q_{ST-BT}/Q_{SC-ST} \tag{16}$$

3.4. Heat Pump

The simulation system uses TRNSYS's own Type941 air-water heat pump. For detailed performance parameters of this heat pump, please refer to its own mathematical model.

The instantaneous COP and annual cumulative COP of HP are:

$$COP_{ihp} = dQ_{HP-BT}/P_{HP} \tag{17}$$

$$COP_{achp} = Q_{HP-BT}/\int_0^{t_7} P_{HP}dt \tag{18}$$

where P_{HP} is the instantaneous power of the HP (W), and t_7 is the annual cumulative number of hours, taking 8760 h.

3.5. System

The total power consumed by SCAHP is:

$$P_t = P_{HP} + P_{pump} + P_{fan} \tag{19}$$

where P_{pump} is the sum of instantaneous powers of all pumps in the system (W), and P_{fan} is the sum of instantaneous power of all fans in the system (W).

The benefits of SCAHP are:

$$Q_{DR} = Q_{BT-DR} \cdot \eta_{AWHE} \tag{20}$$

SCAHP instantaneous COP and annual cumulative COP are:

$$COP_i = dQ_{DR}/P_t \tag{21}$$

$$COP_{ac} = Q_{DR}/\int_0^{t_7} P_t dt \tag{22}$$

3.6. Material Drying Characteristics Analysis

The specific moisture extraction rate can be expressed as (kg/kW h):

$$SMER = (m_{r0} - m_{r2})/\int_0^t P_t dt \tag{23}$$

The dry basis moisture content of the material can be expressed as:

$$M = (m_{r0} - m_{ri})/m_{ri} \tag{24}$$

where m_{ri} is the mass of carrot at time i (kg).

The drying rate can be expressed as:

$$DRa = dM/dt = (M_{t+\Delta t} - M_t)/\Delta t \tag{25}$$

where $M_{t+\Delta t}$ is the moisture content at time $t + \Delta t$ (g moisture/g dry matter), and M_t is the moisture content at time t (g moisture/g dry matter).

3.7. System Economic Analysis

This paper uses the "life cycle" method and the "payback period" method to conduct an economic analysis of SCAHP.

3.7.1. "Life Cycle" Method

Life cycle cost refers to the sum of all expenditures in the entire life cycle of a product, including the acquisition of raw materials, product use costs, etc. It refers to the sum of the production cost of the enterprise and the user's use cost.

The cumulative net value of the dryer life, the cost savings during the life cycle:

$$V_{cnp} = \sum_{t=1}^{t} V_{npt} \tag{26}$$

where V_{npt} is the net present value of the dryer in a period of time calculated by year (t), and the expression is:

$$V_{npt} = \frac{(1+i)^{t-1}}{(1+n)^{t}} \times S_d \times D \tag{27}$$

where i is the inflation rate, taking 0.08, n is the long-term investment interest rate, taking 0.1, D is the number of days the dryer is used per year, and S_d is the money saved per day in a period of time per year $(\mathrm{RMB/d})$. It can be expressed as:

$$S_d = (C_s - C_{ds}) \times m_{r2} \tag{28}$$

where C_s is the selling price of dried carrots $(\mathrm{RMB/d})$, and C_{ds} is the manufacturing cost per kilogram of dried carrots $(\mathrm{RMB/kg})$. It can be expressed as:

$$C_{ds} = C_{fd} + C_d \tag{29}$$

where C_{fd} is the price of fresh carrots required to produce one kilogram of dried carrots $(\mathrm{RMB/kg})$, and C_d is the cost of using a dryer to produce one kilogram of dried carrots $(\mathrm{RMB/kg})$. It can be expressed as:

$$C_{fd} = \frac{m_{r0}}{m_{r2}} C_f \tag{30}$$

where C_f is the price per kilogram of fresh carrots $(\mathrm{RMB/kg})$.

$$C_d = \frac{C_a}{m_{r2} x D} \tag{31}$$

where C_a is the cost of a dryer (RMB). It can be expressed as:

$$C_a = C_{ac} + C_m + C_r \tag{32}$$

where C_{ac} is the annual investment cost of the dryer (RMB), C_m equipment annual maintenance cost (RMB), and C_r is the equipment annual operating cost (RMB). It can be expressed as:

$$C_{ac} = \frac{n(1+n)^{j}}{(1+n)^{j} - 1} \times C_{cc} \tag{33}$$

where C_{cc} is the investment cost of the dryer (RMB), and j is the life of the dryer (year).

The annual operating cost of the system is:

$$C_r = \frac{m_{r0} - m_{ri}}{SMER} \times D \times C_e \tag{34}$$

where C_e is the electricity price per kWh $(\mathrm{RMB/kW\ h})$.

3.7.2. Payback Cycle

The payback period (N) can be expressed as:

$$N = \frac{\ln\left(1 - \frac{C_{cc}}{V_{1pt}}(n-i)\right)}{\ln\left(\frac{1+i}{1+n}\right)} \quad (35)$$

where V_{1pt} is the net present value of the dryer in the first year (RMB).

4. Simulation Model Verification

This study uses the experimental results of Qiu [25] to verify the simulation model. The system parameters are consistent with Qiu. The meteorological parameters adopt the typical meteorological year parameters of Nanjing City. The DR inlet temperature and the DR outlet temperature are the verification objects. As shown in Figure 4, the simulated DR inlet temperature (T_{in-sim}) has an error of 0.07–6.25% compared with the experimental DR inlet temperature (T_{in-exp}), and the average error is 2.36%. Compared with the experimental DR outlet temperature ($T_{out-exp}$), the error of simulated DR outlet temperature ($T_{out-sim}$) is 0.04–10.57%, and the average error is 3.29%.

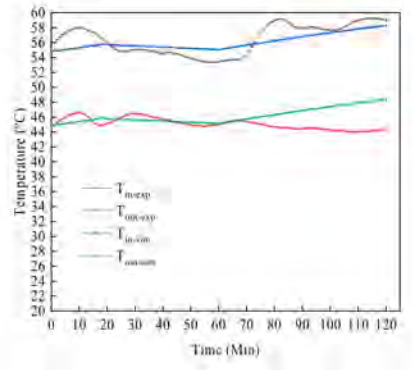

Figure 4. Diagram of comparison and verification of inlet and outlet temperatures of the DR.

Compared with the model proposed by Qiu [25], the model proposed in this paper has an additional air-water heat exchanger that connects the BT and DR. The heat exchanger can be regarded as an efficiency device in essence. As shown in Figure 5, when the heat exchanger efficiency is set to 1, the inlet and outlet temperature of the DR is exactly the same as when the heat exchanger is not installed. Set the heat exchanger efficiency to 0.8, 0.6, 0.4, and get the temperature lines of $T_{in-0.8}$, $T_{out-0.8}$ parallel to T_{in-1}, T_{out-1}. Based on the above comparison and verification results, the simulation system is correct.

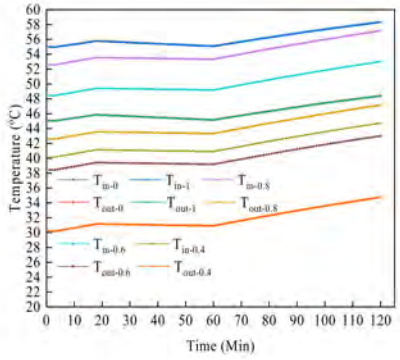

Figure 5. Diagram of verification of the heat exchanger in TRNSYS, essentially an efficiency unit.

5. Results and Discussion

5.1. Variable Air Volume Experiment

In this paper, an electric heating thermostat was modified. On the basis of retaining the original drying room air outlet, a vent was opened, as shown in Figure 6, and a fan added to this vent to perform forced convection for variable air volume experiments and heat recovery. At this time, the original air outlet has become an air inlet, as shown in Figure 7.

Figure 6. Schematic diagram of adding vent to the thermostat.

Figure 7. Schematic diagram of installing fan on vent.

In this experiment, 731 g of fresh carrots were dried in two drying modes: the forced convection fan was turned off mode (TOFF) and the forced convection fan was turned on mode (TONF). The flow rate of the fan is 39 kg/h. The carrots are equally divided into two plates, and the internal dimensions of the incubator are 0.45 m × 0.45 m × 0.4 m. The initial moisture content of drying is 9.15 g moisture/g dry matter, and the final moisture content is 0.25 g moisture/g dry matter. Therefore, when the weight of dry carrot reaches 0.09 kg, the drying process ends. The equipment used in the experiment is shown in Table 4.

Table 4. Basic Parameters of Typical Cities in Five Climate Zones of China.

Equipment	Measuring Range	Accuracy
Electronic scale	0–60 kg	1 g
Electrical parameter tester	0–3500 W	0.1 W
Anemometer	0.3–30 m/s	±3%
Temperature Sensor	−50–200 °C	0.1 °C
Humidity Sensor	1–99%	0.1%

In the experiment, the weight of carrot was measured every half an hour, and the moisture content and drying rate of carrot in the two modes were shown in Figures 8 and 9.

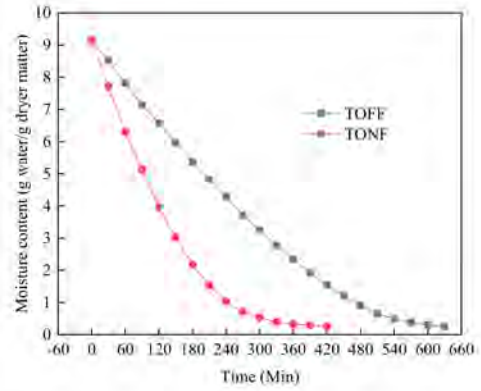

Figure 8. Changes of carrot moisture content with drying time.

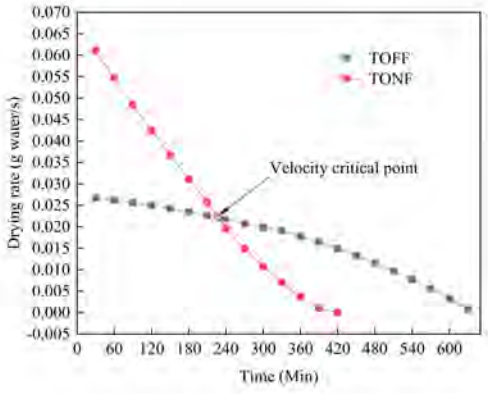

Figure 9. Changes of carrot moisture drying speed with time.

It can be seen from Figure 8 that the drying rate of carrot in the two modes decreases with the increase of time. The drying rate of the TONF mode is 3.5 h faster than that of the TOFF mode, saving 33.3% of the drying time. This is due to the forced convection in the DR, and the humidity is maintained at a low level during the drying process. Natural convection prevents the drying moisture during the drying process from being discharged in time and stays in the DR, making the air humidity close to saturation and inhibiting the drying rate.

It can be seen from Figure 9 that starting from the 4th hour, the drying rate of TONF mode (the forced convection fan was turned on mode) is lower than that of TOFF mode (the forced convection fan was turned off mode). This is because the moisture content of carrots in TONF mode has been reduced to 1.03 g moisture/g dry matter at this time, and the moisture content of the carrots in TOFF mode corresponds to 4.29 g moisture/g dry matter, the latter is much higher than the former, and the lower moisture content of carrots reduces the drying rate.

It can be seen from Figure 10 that the drying energy consumption in TONF mode (the forced convection fan was turned on mode) is 28.26% higher than that in TOFF mode (the forced convection fan was turned off mode). When TONF mode is switched to TOFF mode in the 4th hour, it can save about 20% of energy compared to TONF mode, and only about 8% higher than TOFF mode. In combination with Figures 8–10, we recommend using the mixed mode from TONF to TOFF in the 4th hour (TOCF mode). The drying rate is faster and the energy consumption is low. The following discussion of the article will be based on the TOCF model.

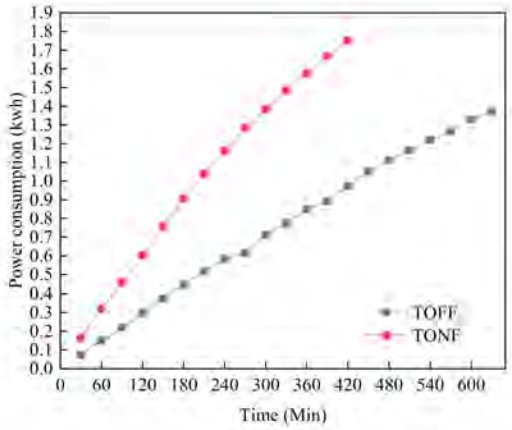

Figure 10. Changes of carrot drying power consumption over time.

5.2. System Optimization

A solar collector (SC) can effectively improve the overall performance of SCAHP. However, due to high initial investment and different climate conditions in various regions, there are certain difficulties in system design. At the same time, as a key component of the system coupling, a hot water storage tank (ST) also has some difficulties in design. There are few researches on the optimization of heat pump drying system configuration. This research tries to give some suggestions.

As shown in Figure 11, the annual cumulative efficiency of the system (COP_{ac}) shows an increasing trend with the increase in the area of solar collector (A_{SC}). This is because as the A_{SC} increases, the proportion of solar heating in the overall heating of the system increases, and the proportion of air-water heat pump (HP) heating is reduced, the total energy consumption of drying room (DR) remains unchanged, the power consumption decreases, and the COP_{ac} increases accordingly. In this configuration, COP_{ac} is 3.571~4.805. As the volume of heat storage water tank (V_{ST}) increases, COP_{ac} gradually slows down as the A_{SC} increases. When the V_{ST} is 0.02 $\sim$ 0.1 m^3, as the A_{SC} increases, the COP_{ac} with a larger V_{ST} system will always surpass the system with a smaller V_{ST} at a certain point. When the V_{ST} is 0.12 $\sim$ 0.4 m^3, as the A_{SC} increases, the COP_{ac} shows an overall downward trend. This is due to the large V_{ST}, the temperature rise of ST is slow, and the heat in the ST cannot be effectively and timely passed to the BT. As a result, on the one hand, the heat collection pump is idling, which increases energy consumption. On the other hand, it cannot effectively reduce the heat supplied by the heat pump and the solar collector cannot be used to the maximum extent, which leads to a decrease in the COP_{ac}.

Figure 11 also reveals that when the A_{SC} is 0.1 $\sim$ 0.25 m^2, the COP_{ac} shows a decreasing trend as the V_{ST} increases, and when the A_{SC} is 0.3 $\sim$ 0.8 m^2, the COP_{ac} increases first and then decreases as the V_{ST} increases; this is because the smaller V_{ST} cannot fully release the heat supply potential of the larger A_{SC}, and as the A_{SC} increases, the V_{ST} corresponding to the highest value of the system efficiency also increases. When A_{SC} is 0.4, 0.5, and 0.6 m^2 correspond to ST with volumes of 0.04, 0.08, and 0.1 m^3, respectively, so that the COP_{ac} reaches the corresponding maximum value. In addition, it can be seen from the figure that when the A_{SC} is 0.1 $\sim$ 0.4 m^2, the distance between the lines is relatively sparse. Within this range, as the A_{SC} increases, the COP_{ac} increases rapidly. When the A_{SC} is 0.45 $\sim$ 0.8 m^2, the distance between the lines is relatively dense. In this range, as the A_{SC} increases, the system efficiency increases slowly, which shows that when the A_{SC} is increased to 0.45 m^2, the system has been mainly heated by the SC, and the HP has played a smaller role. It is recommended to use solar collectors with an area less than 0.45 m^2 in this system.

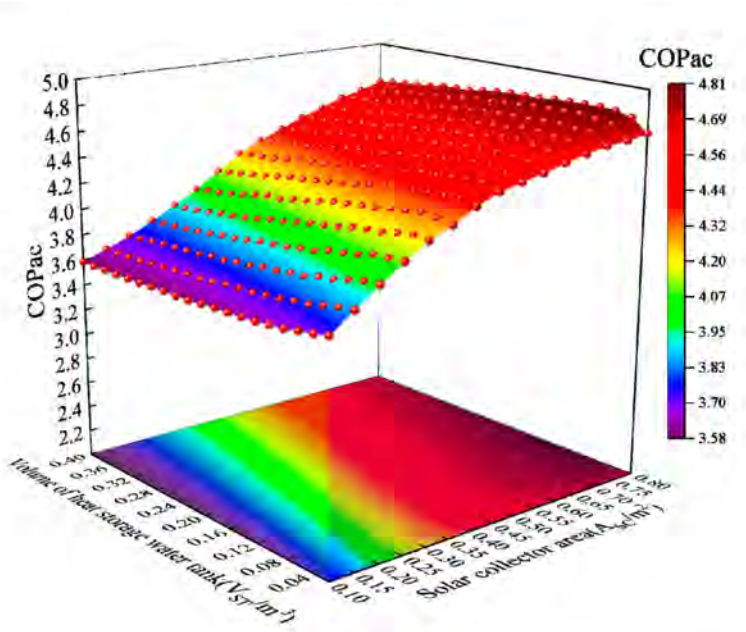

Figure 11. Diagram of COP_{ac} changes as A_{SC} and V_{ST} change.

In summary, the coupling of the SC and ST is very important. Different A_{SC} require designing a ST of appropriate volume. In order to find this appropriate value, we introduce the surface-to-body ratio (SBR): $SBR = A_{op}/(V_{op} + V_{BT})$, Among them, A_{op} and V_{op} respectively represent the A_{SC} and the V_{ST} corresponding to the optimal COP_{ac}. V_{BT} is the volume of BT, taking 0.05 m^3. It can be calculated that the SBR value is concentrated between 3.182~4.091 under the premise of the recommended value.

As shown in Figure 12, when the V_{ST} is 0.02 $\sim$ 0.34 m^3, the η_{ST} increases first and then decreases as the A_{SC} increases. When the V_{ST} is 0.36 $\sim$ 0.4 m^3, the η_{ST} shows an increasing trend as the A_{SC} increases. As the V_{ST} increases, the A_{SC} corresponding to the maximum η_{ST} becomes larger. This is because the larger the V_{ST}, the slower the temperature rise, and a larger A_{SC} is required to provide sufficient heat.

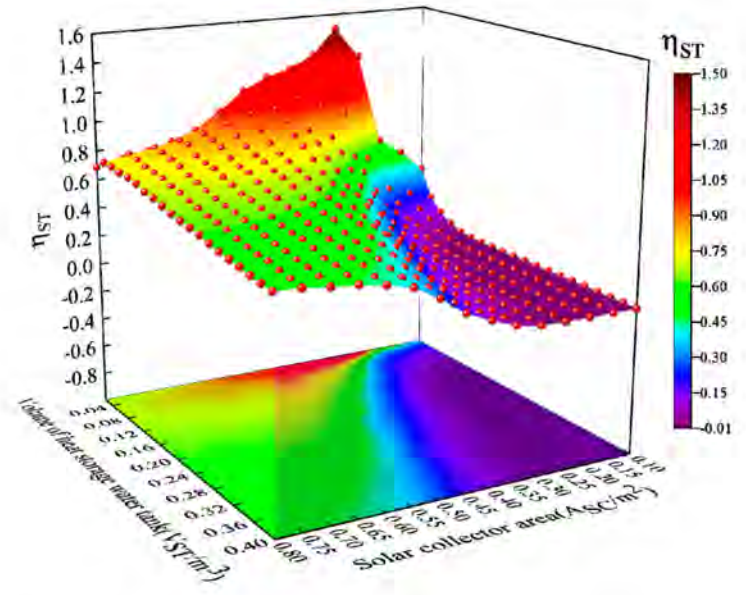

Figure 12. Diagram of η_{ST} changes as A_{SC} and V_{ST} change.

Figure 12 also reveals that when the A_{SC} is 0.1 $\sim$ 0.55 m^2, the η_{ST} shows a decreasing trend as the V_{ST} increases, when the A_{SC} is 0.6 $\sim$ 0.8 m^2, the η_{ST} will first increase and then decrease as the V_{ST} increases. This is because the V_{ST} is too small compared to the A_{SC}, and it cannot store enough solar collector heat. As a result, the heat generated by the SC cannot pass into the BT in time, and the HP needs to be turned on to provide heat to the BT, and the heat generation potential of the SC is not fully utilized. When the A_{SC} is 0.45 $\sim$ 0.8 m^2, the distance between the lines is relatively dense. In this range, as the V_{ST} increases, the η_{ST} decreases slowly. This shows that when the A_{SC} increases to 0.45 m^2, it is enough to meet the energy demand of the system. The decrease in the η_{ST} is mainly caused by the increase in V_{ST}. This shows that more heat from the SC is wasted, which confirms the analysis result in Figure 11.

To sum up, take the η_{ST} as the goal, and based on the effective value of this calculation, the best SBR can be calculated from 1.923 to 4.444, and the A_{SC} corresponding to the maximum η_{ST} is greater than 0.3 m^2. It can be seen that the η_{ST} does not match the overall efficiency of the system. It is recommended to choose a small V_{ST} after selecting the A_{SC}, and increase the η_{ST} to avoid too much heat from the solar collector being wasted. Combining increasing the A_{SC} and V_{ST} will also increase the initial investment, and it is recommended not to take the η_{ST} as the first choice for system design.

As shown in Figure 13, the η_{BT} shows a trend of increasing first and then decreasing as the A_{SC} increases; this is because when the A_{SC} is relatively small, the heat of the BT comes from the HP.The HP heats the BT to 65 °C, and during the process of lowering the temperature of the BT, the heat loss is large, which causes the η_{BT} to be low. As the A_{SC} increases, the heat received by the BT from the SC increases, and the BT will no longer rise to 65 °C frequently, thereby reducing heat loss and improving η_{BT}. With the further increase in the A_{SC}, enough heat can be stored in the ST. When the system shuts down at night, the heat from the ST will be transferred to the BT, and then it will interact with the surrounding atmosphere in the BT. The heat exchange causes waste, and the η_{BT} is gradually reduced. This problem will be solved in a non-stop system.

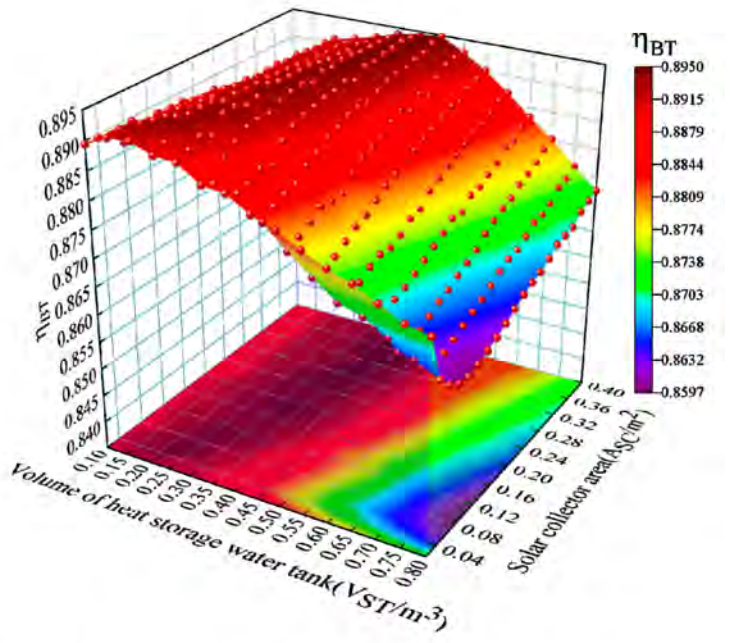

Figure 13. Diagram of η_{BT} changes as A_{SC} and V_{ST} change.

Figure 13 also reveals that when the A_{SC} is 0.1 $\sim$ 0.45 m^2, the η_{BT} shows a basically unchanged trend with the increase of V_{ST}, during the whole process, the η_{BT} changes at most by 1.49% and at least 0.44%, which can be ignored. This is because the SC cannot provide sufficient heat for the BT to lose heat at night. When the A_{SC} is 0.5 $\sim$ 0.8 m^2, the η_{BT} decreases first and then increases as the V_{ST} increases, this is because SC can provide sufficient heat at this time, the ST has a small volume and a high temperature. When it is shut down at night, the ST can provide more heat to the BT, resulting in greater heat loss, as the V_{ST} increases, the temperature of the ST decreases the amount of heat transfer is reduced, the heat loss is also reduced, and the heating efficiency of the BT is gradually improved. In summary, the system configuration required for the maximum efficiency of the BT is different from the system configuration required for the maximum efficiency of the ST.

As shown in Figure 14, the heat provided by the SC shows an increasing trend as the A_{SC} increases. When the A_{SC} is 0.1 $\sim$ 0.65 m^2, the heat supply of the SC shows an increasing trend as the V_{ST} increases, when the A_{SC} is 0.7 $\sim$ 0.8 m^2, the heat supply of SC will decrease first and then increase as the V_{ST} increases. This is because when the A_{SC} is small, as the V_{ST} increases, it can absorb more heat from the SC, and when the A_{SC} is larger, the smaller V_{ST} quickly heats up, which can make better use of the heat recovered from the waste heat, causing the SC to decrease the heat first. The heat provided by the HP shows a decreasing trend as the A_{SC} increases, when the A_{SC} is 0.1 $\sim$ 0.25 m^2, the heat supply of the HP shows an increasing trend as the V_{ST} increases, when the A_{SC} is 0.3 $\sim$ 0.8 m^2, the heat supply of the HP decreases first and then increases as the V_{ST} increases; this is because when the A_{SC} is 0.1 $\sim$ 0.25 m^2, the system mainly relies on the HP heating. As the A_{SC} increases, the system mainly uses the SC for heating, the heat supplied by the HP decreases in the initial stage. Later, as the V_{ST} increases, the η_{ST} decreases, and the BT needs the HP to provide more heat, which is consistent with the analysis in Figure 12. When the A_{SC} is 0.15 $\sim$ 0.35 m^2, the heat supply ratio of the SC is 34.14~68.03%, which is reasonable.

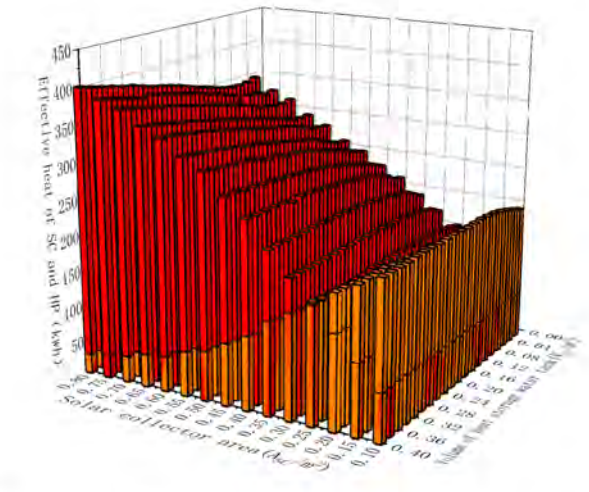

Figure 14. Diagram of the effective heat provided by the SC and HP as A_{SC} and V_{ST} change.

Based on the above analysis, water tank efficiency and heat supply analysis, we suggest that the A_{SC} of this system is 0.15 $\sim$ 0.35 m^2, the SBR is between 3.2~4.1, and the V_{ST} is 0.02 $\sim$ 0.06 m^3. The recommended values for other climate zones are shown in Table 5. The following analysis in this paper will be based on Nanjing, with a A_{SC} of 0.3 m^2 and a V_{ST} of 0.04 m^3.

Table 5. Recommendation system configuration parameter table of other typical cities.

Name	Recommended SBR	The Recommended Value of I_{SC} Is Unchanged throughout the Year (°)	The Recommended Value of I_{SC} Varies throughout the Year (°)
Harbin	1.43~2.78	40	50/40 [1]
Tianjin	1.43~3.57	35	50/30 [1]
Guangzhou	2.14~3.33	20	40/15 [1]
Kunming	1.43~2.86	25	45/20 [1]

[1] a/b means that the I_{SC} is changed to a° in March, and the I_{SC} is changed to b° in November until March of the following year.

As shown in Figure 15a, the difference in heat supplied by the SC with different I_{SC} in 12 months ranges from 4.83 to 58.27%. October is the month with the smallest difference and June is the month with the largest difference, and the annual average difference is 23.2%. It can be seen that the design of the I_{SC} plays a key role. The annual heat provided by the SC increases first and then decreases with the increase of the I_{SC}. When the I_{SC} is 30°, the total heat provided by the SC throughout the year is the largest. If the SC is designed to have no tilt angle change throughout the year, it is recommended to select a tilt angle of 30°.

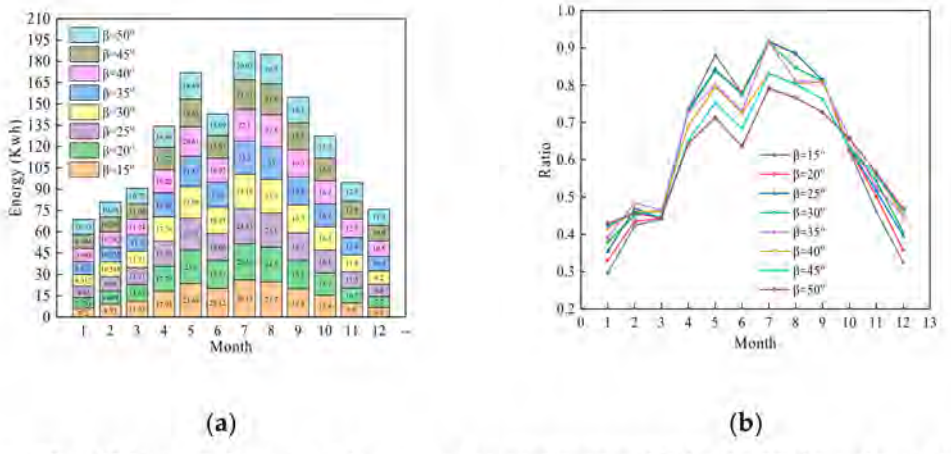

Figure 15. (**a**) Schematic diagram of the energy that can be provided by the SC throughout the year under different I_{SC}. (**b**) Schematic diagram of the ratio of heat provided by the SC in the total heat supply of the system under different I_{SC}.

As shown in Figure 15b, when Nanjing is in January to February and November to December, and the I_{SC} is 50°, the most heat is collected. From March to October, the solar collector can collect the most heat when the I_{SC} is 15°. Therefore, we recommend changing the I_{SC} twice a year. In March, change the I_{SC} to 50°, and in November Change the I_{SC} to 15° until March of the next year. The configuration parameters of I_{SC} in other cities are shown in Table 5.

5.3. Economic Analysis

The price of material is an important factor affecting the economic analysis of the drying system. According to the heat conservation relationship and calculation, using the life cycle method, the total amount of dried carrot in the system throughout the year is 45.99 kg. Table 6 shows the annual net present value of Nanjing and the cumulative net present value of the system life. The life cycle method is used to determine the dry payback period of carrot as 5 years. The cumulative net present value is 13,654 yuan respectively.

Table 6. Annual revenue diagram of Nanjing drying system.

Year	Annual Net Present Worth	Cumulative Net Present Worth
1	808.17	808.17
2	793.48	1601.65
3	779.05	2380.7
4	764.88	3145.58
5	750.98	3896.56
6	737.32	4633.88
7	723.91	5357.79
8	710.76	6068.55
9	697.83	6766.38
10	685.14	7451.52
11	672.69	8124.21
12	660.46	8784.67
13	648.45	9433.12
14	636.66	10,069.78
15	625.08	10,694.86
16	613.71	11,308.57
17	602.56	11,911.13
18	591.6	12,502.73
19	580.84	13,083.57
20	570.28	13,653.85

6. Conclusions

The energy analysis of SCAHP is carried out. The energy coupling relationship of the system in different climate regions is established, and the optimization model of the system is discussed. It can be concluded:

(1) It is recommended to use the mixed variable air volume mode (TOCF mode) for drying, which can save about 20% of the drying time;
(2) The system configuration to achieve the maximum system efficiency is not consistent with the system configuration to achieve the maximum water tank efficiency. It is suggested to choose a smaller V_{ST} after selecting A_{SC} to increase the heating efficiency of the ST and improve the system energy utilization rate.
(3) It is suggested that the SBR of SCAHP in Nanjing should be between 3.182 and 4.091, and I_{SC} should be changed twice a year. In March, I_{SC} should be changed to 50°, and in November, I_{SC} should be changed to 15° until the following March. The configuration parameter recommendations for the other cities are shown in Table 5.
(4) Taking Nanjing as an example to analyze the economy of SCAHP, it can be concluded that the recovery cycle is 5 years, and the system is economically feasible.

Author Contributions: Conceptualization, Z.X. and Y.G.; methodology, Z.X.; software, Z.X. and C.Y.; validation, Z.X. and C.Y.; formal analysis, Y.Y. and Y.L.; investigation, Y.Y. and Y.L.; writing—original draft preparation, Z.X.; writing—review and editing, Z.X. and Y.G. All authors have read and agreed to the published version of the manuscript.

Funding: This research was funded by Guangzhou Science and Technology Plan Project, grant number 201903010068, Science and Technology Service Network Initiative of Chinese Academy of Sciences, grant number KFJ-STS-QYZX-114 and KFJ-STS-QYZD-2021-02-006, Tianjin key research and development project, grant number 20YFYSGX00020.

Institutional Review Board Statement: Not applicable.

Informed Consent Statement: Not applicable.

Data Availability Statement: Not applicable.

Acknowledgments: Thanks to others in the author's research group for their support in this work.

Conflicts of Interest: The authors declare that there is no conflict of interest.

Nomenclature

SCAHP	solar assisted heat pump drying system with waste heat recovery
SC	solar collector
BT	buffer tank
ST	hot water storage tank
HP	air-water heat pump
DR	drying room
AWEH	air-water heat exchanger
TONF	the turn on fan mode
TOFF	the turn off fan mode
SBR	surface-to-body ratio, m^{-1}
COP_{ac}	the annual cumulative efficiency of the system
η_{BT}	buffer tank heating efficiency
η_{ST}	hot water storage tank heating efficiency
q_{DR}	hot air volume, kg/h
A_{SC}	area of solar collector, m^2
I_{SC}	inclination angle of solar collector, ^{o}
V_{ST}	volume of heat storage water tank, m^3
T_{BT}	the average temperature of buffer tank, °C
T_{ST}	the outlet temperature of hot water storage tank, °C
$T_{SC\text{-}IN}$	the inlet temperature of solar collector, °C
$T_{SC\text{-}OUT}$	the outlet temperature of solar collector, °C
$T_{in\text{-}exp}$	The inlet temperature of the drying room obtained from the Qiu experiment
$T_{out\text{-}exp}$	The outlet temperature of the drying room obtained from the Qiu experiment
$T_{in\text{-}sim}$	The inlet temperature of the drying room obtained by simulation
$T_{out\text{-}sim}$	The outlet temperature of the drying room obtained by simulation
$T_{in\text{-}1/0.8/\cdots}$	When the heat exchanger efficiency is 1, 0.8, 0.6, ⋯, the simulated drying room inlet temperature
$T_{out\text{-}1/0.8/\cdots}$	When the heat exchanger efficiency is 1, 0.8, 0.6, ⋯, the simulated drying room outlet temperature

References

1. Mohanraj, M.; Belyayev, Y.; Jayaraj, S.; Kaltayev, A. Research and developments on solar assisted compression heat pump systems—A comprehensive review (part-B: Applications). *Renew. Sustain. Energy Regen.* **2018**, *83*, 124–155. [CrossRef]
2. Hao, W. Theoretical and Experimental Research on the Dual Working Medium Drying System Based on Solar Energy Thermal Utilization. Ph.D. Thesis, Shandong University, Jinan, China, 2020.
3. Mujumdar, A.S. *Handbook of Industrial Drying*, 3rd ed.; CRC Press: Boca Raton, FL, USA, 2006; pp. 2–29.
4. Colak, N.; Hepbasli, A. A review of heat pump drying: Part 1—Systems, models and studies. *Energy Convers. Manag.* **2009**, *50*, 2180–2186. [CrossRef]
5. Lawton, J. Drying: The role of heat pumps and electromagnetic fields. *Phys. Technol.* **1978**, *9*, 214–220. [CrossRef]
6. Queiroz, R.; Gabas, A.L.; Telis, V.R.N. Drying kinetics of tomato by using electric resistance and heat pump dryers. *Dry Technol.* **2004**, *22*, 1603–1620. [CrossRef]
7. Claussen, I.C.; Ustad, T.S.; Strmmen, I.; Walde, P.M. Atmospheric freeze drying—A review. *Dry Technol.* **2007**, *25*, 947–957. [CrossRef]
8. Krokida, M.K.; Kiranoudis, C.T.; Maroulis, Z.B.; Marinos-Kouris, D. Drying related properties of apple. *Dry Technol.* **2000**, *18*, 1251–1267. [CrossRef]
9. Perera, C.O.; Rahman, M.S. Heat pump dehumidifier drying of food. *Trends Food Sci. Technol.* **1997**, *8*, 75–79. [CrossRef]
10. Prasertsan, S.; Saen-saby, P. Heat pump drying of agricultural materials. *Dry Technol.* **1998**, *16*, 235–250. [CrossRef]
11. Rossi, S.; Neues, L.; Kicokbusch, T. Thermodynamic and energetic evaluation of a heat pump applied to the drying of vegetables. *Drying* **1992**, *92*, 1475–1478.
12. Hodgett, D. Efficient drying using heat pumps. *Chem. Energy* **1976**, *311*, 510–512.
13. Geeraert, B. Air drying by heat pumps with special reference to timber drying. In *Heat Pumps and Their Contribution to Energy Conservation*, 1st ed.; Camatini, E., Kester, T., Eds.; Springer: Berlin/Heidelberg, Germany, 1976; pp. 219–246.
14. Hawlader, M.N.A.; Perera, C.O.; Tian, M.; Yeo, K.L. Drying of guava and papaya: Impact of different drying methods. *Dry Technol.* **2006**, *24*, 77–87. [CrossRef]
15. Sun, Z.; Wang, Q.; Xie, Z.; Liu, S.; Su, D.; Cui, Q. Energy and exergy analysis of low GWP refrigerants in cascade refrigeration system. *Energy* **2019**, *170*, 1170–1180. [CrossRef]

16. Wang, N.; Ye, Q.; Chen, L.; Zhang, H.; Zhong, J. Improving the economy and energy efficiency of separating water/acetonitrile/isopropanol mixture via triple-column pressure-swing distillation with heat-pump technology. *Energy* **2021**, *215*, 119–126. [CrossRef]
17. Li, X.; Wang, D. Study on thermodynamic characteristics of multi-unit parallel heat pump drying System. *Chin. J. Refrig. Technol.* **2018**, *38*, 61–67.
18. Hasan Ismaeel, H.; Yumrutaş, R. Investigation of a solar assisted heat pump wheat drying system with underground thermal energy storage tank. *Sol. Energy* **2020**, *199*, 538–551. [CrossRef]
19. Fudholi, A.; Sopian, K.; Ruslan, M.H.; Alghoul, M.A.; Sulaiman, M.Y. Review of solar dryers for agricultural and marine products. *Renew. Sustain. Energy Regen.* **2010**, *14*, 1–30. [CrossRef]
20. El-Sebaii, A.A.; Shalaby, S.M. Solar drying of agricultural products: A review. *Renew. Sustain. Energy Regen.* **2012**, *16*, 37–43. [CrossRef]
21. Huilong, L.; Jinhui, P.; Libo, Z.; Shenghui, G. Performance analysis of a solar energy drying system in conjunction with air source heat pump. *Acta Energy Sol. Sin.* **2012**, *33*, 963–967.
22. Rahman, S.M.A.; Saidur, R.; Hawlader, M.N.A. An economic optimization of evaporator and air collector area in a solar assisted heat pump drying system. *Renew. Sustain. Energy Regen.* **2013**, *76*, 377–384. [CrossRef]
23. Koşan, M.; Demirtaş, M.; Aktaş, M.; Dişli, E. Performance analyses of sustainable PV/T assisted heat pump drying system. *Sol. Energy* **2020**, *199*, 657–672. [CrossRef]
24. Laszlo, L. Solar drying. In *Handbook of Industrial Drying*, 3rd ed.; Mujumdar, A.S., Ed.; CRC Press: Boca Raton, FL, USA, 2006; Volume 2, pp. 304–346.
25. Qiu, Y.; Li, M.; Hassanien, R.H.E.; Wang, Y.; Luo, X.; Yu, Q. Performance and operation mode analysis of a heat recovery and thermal storage solar-assisted heat pump drying system. *Sol. Energy* **2016**, *137*, 225–235. [CrossRef]
26. Wang, Y.; Li, M.; Qiu, Y.; Yu, Q.; Luo, X.; Li, G. Performance analysis of a secondary heat recovery solar-assisted heat pump drying system for mango. *Energy Explor. Exploit.* **2019**, *37*, 1377–1387. [CrossRef]